In vivo, real-time, transnasal, image-guided Raman endoscopy: defining spectral properties in the nasopharynx and larynx

Mads Sylvest Bergholt
Kan Lin
Wei Zheng
David Pang Cheng Lau
Zhiwei Huang

In vivo, real-time, transnasal, image-guided Raman endoscopy: defining spectral properties in the nasopharynx and larynx

Mads Sylvest Bergholt,[a] **Kan Lin,**[a] **Wei Zheng,**[a] **David Pang Cheng Lau,**[b] **and Zhiwei Huang**[a]
[a]National University of Singapore, Optical Bioimaging Laboratory, Department of Bioengineering, Faculty of Engineering, Singapore
[b]Singapore General Hospital, Department of Otolaryngology, Singapore

Abstract. We report for the first time the implementation of transnasal, image-guided Raman endoscopy to directly assess Raman spectral properties of nasopharyngeal and laryngeal tissue *in vivo* during clinical endoscopic examinations. A rapid 785-nm excitation Raman endoscopy system, coupled with a miniaturized fiber-optic Raman probe, was utilized for real-time, *in vivo* Raman measurements of different anatomical locations in the head and neck. A total of 874 high-quality *in vivo* Raman spectra were successfully acquired from different anatomic locations of the nasopharynx and larynx [i.e., posterior nasopharynx (PN) ($n = 521$), the fossa of Rosenmüller (FOR) ($n = 157$), and true laryngeal vocal chords (LVC) ($n = 196$)] in 23 normal subjects at transnasal endoscopy. Difference spectra and principal component analysis (PCA) were employed for tissue characterization, uncovering the tissue variability at the biomolecular level. The PCA-linear discriminant analysis (LDA) provides sensitivity of 77.0% and specificity of 89.2% for differentiation between PN and FOR, and sensitivity of 68.8% and specificity of 76.0% for distinguishing LVC and PN using the leave-one-subject-out, cross-validation method. This work demonstrates that transnasal, image-guided Raman endoscopy can be used to acquire *in vivo* Raman spectra from the nasopharynx and larynx in real time. Significant Raman spectral differences ($p < 0.05$) identified as reflecting the distinct composition and morphology in the nasopharynx and larynx should be considered to be important parameters in the interpretation and rendering of diagnostic decision algorithms for *in vivo* tissue diagnosis and characterization in the head and neck. © *2012 Society of Photo-Optical Instrumentation Engineers (SPIE).* [DOI: 10.1117/1.JBO.17.7.077002]

Keywords: *in vivo* diagnosis; Raman endoscopy; larynx; nasopharynx; head and neck.

Paper 12102 received Feb. 15, 2012; revised manuscript received May 31, 2012; accepted for publication Jun. 6, 2012; published online Jul. 9, 2012; corrected Jul. 25, 2012.

1 Introduction

Head and neck malignancies, including laryngeal and nasopharyngeal cancers, are diseases with high mortality rates.[1] In East Asia and Africa, the rates of incidence and mortality due to nasopharyngeal carcinomas (NPCs) and laryngeal cancer are remarkably higher than many parts of the world.[2] The five-year survival rate decreases significantly due to delayed diagnosis and NPC symptoms that are generally present at late tumor-node-metastasis. Early identification and adequate preoperative assessment of both NPCs and laryngeal cancers allow functional preserving therapy (e.g., radiation therapy, chemotherapy, surgery, etc.) and are also critical to reducing the mortality rates of the patients. Yet, early diagnosis of nasopharyngeal and laryngeal precancer and early cancer is clinically challenging, even for experienced clinicians with the aid of conventional white-light reflectance (WLR) endoscopy (e.g., microlaryngoscopy, transnasal esophagoscopy).[3] Positive identification of these lesions relies heavily on the visualization of gross morphological manifestations, which can be very subjective. Therefore, it would be of imperative clinical value to develop a real-time, biomolecular-sensitive optical diagnostic technology ("optical biopsy") that can assist in the early detection of nasopharyngeal

and laryngeal dysplasia and neoplasia during transnasal endoscopic inspections.

In recent years, near-infrared (NIR) Raman spectroscopy has shown promising results for the pointwise diagnosis and characterization of disease progression in various organs (e.g., gastrointestinal tracts,[4–13] oral cavity,[14] nasopharynx[15,16], larynx,[15,17–19] lung,[20] cervix,[21,22] bladder,[23] skin,[24,25] and breast[26]) with high biomolecular specificity. To date, NIR Raman spectroscopic studies on the nasopharynx and larynx have been limited to *in vitro* tissue Raman measurements due to the lengthy data acquisition times, as well as technical challenges in making miniaturized flexible fiber-optic Raman probes with high collection efficiencies while also effectively eliminating interferences from fluorescence and silica Raman signals.[27] The diagnostic sensitivities and specificities of ∼70% to 95% have been achieved in differentiating between different laryngeal pathologic types (e.g., normal, dysplasia and carcinoma) *in vitro* using NIR Raman spectroscopy.[19] Teh et al. reported a diagnostic sensitivity of 88.0% and specificity of 91.4% for detecting laryngeal carcinoma *in vitro* when coupled with random recursive partitioning ensemble techniques.[18] Lau et al. confirmed the feasibility of nasopharyngeal and laryngeal cancer diagnosis *in vitro*.[16,17] Very recently, we have initiated a targeted study aiming to translate the Raman spectroscopy technology from laboratory into routine, real-time, clinical endoscopic diagnostics, and have succesfully demonstrated the applications of

Address all correspondence to: Zhiwei Huang, National University of Singapore, Optical Bioimaging Laboratory, Department of Bioengineering, Faculty of Engineering, Singapore. Tel: 65-6516-8856; Fax: 65-6872-3069; E-mail: biehzw@nus.edu.sg

Raman endoscopy for real-time *in vivo* diagnosis of upper gastrointestinal (i.e., esophageal and gastric) dysplasia and neoplasia.[11–13] With our successful development of a 1.8-mm Raman fiber probe that can pass down the instrument channel of medical endoscopes,[27] this allowed us to evaluate the clinical merit of the transnasal Raman endoscopy technique for *in vivo* tissue characterization in the head and neck. Since the compositional and morphological profiles of different organs (i.e., larynx and nasopharynx) in the head and neck are highly functionally specialized and exhibit significant variations in anatomical and morphological properties (e.g., lymphoid tissues, vascularity, secretion, cartilage, etc.), there is a fundamental ambiguity to which extent one may account for inter-anatomical variabililty in developing efficient algorithms for *in vivo* nasopharyngeal and laryngeal tissue Raman diagnostics. In this study, we report for the first time the implementation of transnasal image-guided Raman endoscopy [i.e., WLR and narrowband imaging (NBI)] to directly assess and characterize distinctive Raman spectral properties of nasopharyngeal and laryngeal tissue *in vivo*. Raman spectral differences reflecting the distinct composition and morphology among the nasopharynx and larynx are further evaluated using multivariate techniques [i.e., principal components analysis (PCA) and linear discriminant analysis (LDA)].

2 Materials and Methods

2.1 *Raman Endoscopy Platform*

The unique, image-guided Raman endoscopy platform developed for *in vivo* tissue measurements and characterization has been described in detail elsewhere.[27] Briefly, the Raman spectroscopy system consists of a spectrum-stabilized, 785-nm diode laser (maximum output: 300 mW, B&W TEK Inc., Newark, DE), a transmissive imaging spectrograph (Holospec $f/1.8$, Kaiser Optical Systems, Ann Arbor, MI) equipped with a liquid nitrogen-cooled ($-120°C$), NIR-optimized, back-illuminated, and deep depletion charge-coupled device (CCD) camera (1340×400 pixels at 20×20 μm per pixel; Spec-10: 400BR/LN, Princeton Instruments, Trenton, NJ). The novel spectrometer fiber input coupling consists of parabolic aligned array of 58 fibers (100 μm) to correct the spectrometer image aberration for improving both the spectral resolution and signal-to-noise ratio of Raman signals.[28] We have constructed a 1.8-mm fiber-optic Raman probe for transnasal endoscopic applications, maximizing both the tissue excitation and *in vivo* tissue Raman collections. The Raman fiber probe fits into the instrument channel of flexible transnasal endoscopes and can be safely directed to different locations in the nasopharynx and larynx under wide field imaging (i.e., WLR and NBI) guidance. The clinical Raman endoscopy platform has been integrated with our recently developed online data processing software to facilitate probe handling advice and sound feedback to clinicians in real time (processing time <0.1 s). Briefly, the online Raman endoscopy framework synchronizes spectral acquisition (i.e., laser exposure, integration time, CCD shutter and readout, etc.) and automatically extracts the Raman signals from the raw tissue spectra (comprising strong autofluorescence background and weak Raman signals) using established preprocessing methods such as smoothing, fifth-order polynomial baseline subtraction, etc.[27] The *in vivo* Raman spectra and the outcome of multivariate algorithms (e.g., PCA) can be displayed in real time in a

comprehensible graphical user interface (GUI) during clinical transnasal Raman endoscopy.[21]

2.2 *Subjects*

A total of 23 normal healthy male subjects of different races (22 Asian and 1 Caucasian) were recruited for *in vivo* tissue Raman measurements with transnasal endoscopy. In these subjects, no suspicious lesions were identified under the WLR and NB imaging examination. A total of three primary measurement sites of assumed normal (or benign) tissues were predefined for *in vivo* Raman acquisitions, including the true laryngeal vocal cords (LVCs), the posterior nasopharynx (PN), and the pharyngeal recess [i.e., fossa of Rosenmüller (FOR)] where NPC typically initiates. The fiber-optic Raman probe can be placed in gentle contact with internal tissues interrogating with the endogenous biomolecular compositions of tissue in real time. The accurate positioning against the tissue sites measured was verified on the WLR/NBI monitor by the endoscopists in charge. The probe allowed Raman spectra to be collected from an area (200 μm in diameter) with probing volume of approximately 1 mm³ and penetration depth of $\sim$800 μm. Each spectrum was acquired within 0.5 s using the 785-nm laser light with the power of $\sim$50 mW on the tissue surface.[12,29] The Raman spectra were displayed online and were stored for postprocedural inspection. This rapid Raman endoscopic technology is nondestructive and can now be used routinely under endoscopic transnasal examinations for clinical evaluation. To assess the intra-tissue site variance, several Raman spectra ($\sim$18) were also acquired from each tissue site. As a result, a total of 874 *in vivo* Raman spectra from 47 sites were measured with transnasal endoscopy and used for spectral analysis [PN ($n = 521$), FOR ($n = 157$) and LVC ($n = 196$)] from the 23 subjects.

2.3 *Multivariate Statistical Analysis*

This study aims to characterize the Raman spectral properties of different locations in the head and neck and to transfer Raman spectroscopy from bench into transnasal endoscopic applications. Prior to data analysis, the raw Raman spectra were smoothed using a linear Savitzky-Golay filter, and the tissue autofluorescence background was then subtracted from the smoothed spectra using a fifth-order polynomial fit. The background-subtracted Raman spectra were normalized to the integrated areas under the curves to minimize the effect of Raman probe-handling variations on clinical Raman measurements with respect to different subjects and tissue sites. All processed Raman spectra were assembled into a matrix, and the mean centering of the entire Raman dataset was then performed. To reduce the dimension of the spectral data, PCA was employed to extract a set of orthogonal principal components (PCs) that account for the maximum variance in the Raman spectral dataset for tissue characterization.[5,22] Accordingly, loadings on the PCs represent orthogonal basis spectra of the most prominent spectral variation in the dataset accounting for progressively decreasing variance, whereas the scores on the PCs represent the projection value of the tissue Raman spectra on the corresponding loading. Thus, PCA can efficiently be used to resolve spectral variations while reducing the dimension of the dataset to a minimum.[22] The number of retained PCs was chosen based on the analysis of variance (ANOVA) and Student's *t*-test at 0.05 level. We employed *post hoc* Fisher's

least-squares differences (LSD) test[11] to assess differences in means. Multivariate statistical analysis was performed using the PLS toolbox (Eigenvector Research, Wenatchee, WA) in the Matlab (Mathworks Inc., Natick, MA) programming environment.

3 Results

High-quality *in vivo* Raman spectra can routinely be acquired in the nasopharynx and larynx in real time during transnasal image-guided [i.e., WLR and NBI] endoscopic inspections. Figure 1 shows an example of *in vivo* raw Raman spectrum (a weak Raman signal superimposed on a large-tissue autofluorescence background) acquired from the PN with an acquisition time of 0.1 s at endoscopy. The background-subtracted tissue Raman spectrum with a signal-to-noise ratio (SNR) of >10 (see the inset of Fig. 1) can be obtained and displayed online during clinical endoscopic measurements. Figure 2 depicts the inter-subject *in vivo* mean Raman spectra ±1 standard deviation (SD) of normal nasopharyngeal [PN ($n = 521$) and FOR ($n = 157$)] and laryngeal tissues [LVC ($n = 196$)] when the Raman probe is gently put in contact with the tissue under WLR/NB imaging guidance. Also shown is WLR images obtained from the corresponding anatomical locations. Prominent Raman bands associated with proteins and lipids are identified as shown in Table 1 with tentative biomolecular assignments.[5,11,13,20,30] Figure 3 shows the intra-subject mean spectra ±1 SD of a randomly chosen subject. The *in vivo* tissue Raman spectra were found to be reproducible with diminutive inter- and intra-subject variances (<10%) in the nasopharynx and larynx. Further Raman endoscopic testings indicate that the variability between different tissue sites within the PN is very subtle (Raman intensity variations of <5%; data not shown). We also calculated difference spectra ±1 SD between different tissue types (i.e., PN-LVC, LV-FOR, and PN-FOR) as shown in Fig. 4, resolving the distinctive compositional and morphological profiles of different anatomical tissue sites at the biomolecular level. ANOVA revealed 12 prominent and broad Raman spectral subregions that showed significant variability ($p < 0.0001$) among the three anatomical tissue sites centered at 812, 875, 948, 986, 1,026, 1,112, 1,254, 1,340, 1,450,
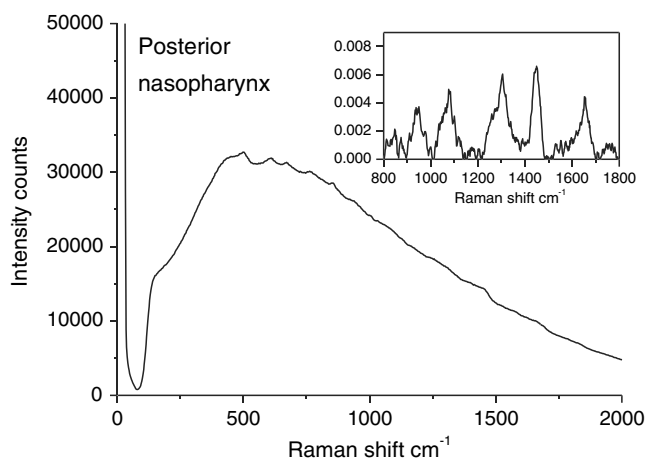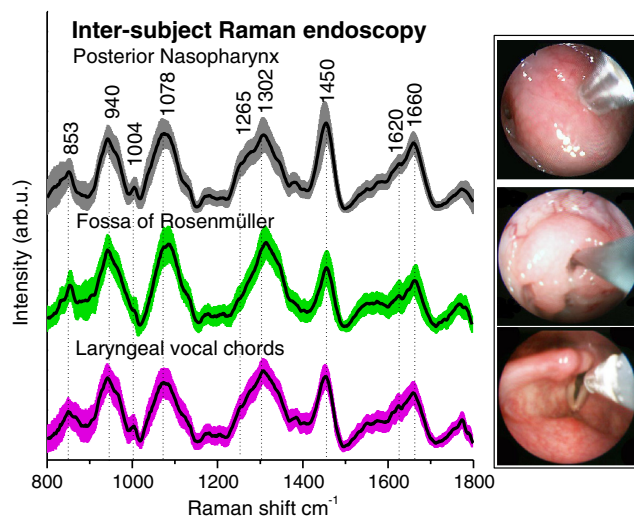
Fig. 2 *In vivo* (inter-subject) mean Raman spectra ±1 SD of PN ($n = 521$), FOR ($n = 157$) and LVCs ($n = 196$). Note that the mean Raman spectra are vertically displaced for better visualization. *In vivo*, fiber-optic Raman endoscopic acquisitions from PN (upper), FOR (mid), and LVCs (lower) under WLR and NB imaging guidance are also shown.

1,558, 1,655, and 1,745 cm^{-1}, reconfirming the importance of characterizing the Raman spectral properties of nasopharynx and larynx toward accurate *in vivo* tissue diagnostics.

To investigate the significance of potential confounding factors during transnasal endoscopy, we also measured *in vitro* Raman spectra of blood, saliva, and nasal mucus obtained from healthy volunteers, as shown in Fig. 5. The most prominent Raman bands in saliva and nasal mucus are at 1638 cm^{-1} (v_2 bending mode of water), whereas blood exhibits porphyrin Raman bands near 1560 and 1620 cm^{-1}.[31] To assess further the spectral differences among different tissues in the head and neck, a five-component PCA model based on ANOVA and Student's *t*-test ($p < 0.05$) accounting for 57.41% of the total variance (PC1: 22.86%; PC2: 16.16%; PC3: 8.13%; PC4 6.22% PC5: 4.04%) was developed to resolve the significant peak variations of different anatomical locations. Figure 6 shows the PC loadings revealing the Raman bands associated with proteins (i.e., 853, 940, 1004, 1265, 1450, and 1660 cm^{-1}) and lipids (i.e., 1078, 1302, 1450, 1655, and 1745 cm^{-1}). Figure 7 displays box charts of PCA scores for the different tissue types (i.e., PN, FOR, and LVC). The line within each notch box represents the median, and the lower and upper boundaries of the box indicate first (25.0% percentile) and third (75.0% percentile) quartiles, respectively. Error bars (whiskers) represent the 1.5-fold interquartile range. The *p*-values are also represented among different tissue types. Dichotomous PCA algorithms integrated with LDA provided the sensitivities of 77.0% (401/521), 68.8% (132/192) and specificities of 89.2% (140/157) and 76.0% (396/521) for differentiation between PN and FOR and between LVC and PN, respectively, using the leave-one-subject-out (LOSO), cross-validation method. Overall, these results demonstrate that Raman spectra of nasopharynx and larynx in the head and neck can be measured *in vivo* with transnasal endoscopy, and the diagnostic algorithms development should be tissue site–specific to ensure minimum algorithm complexity.
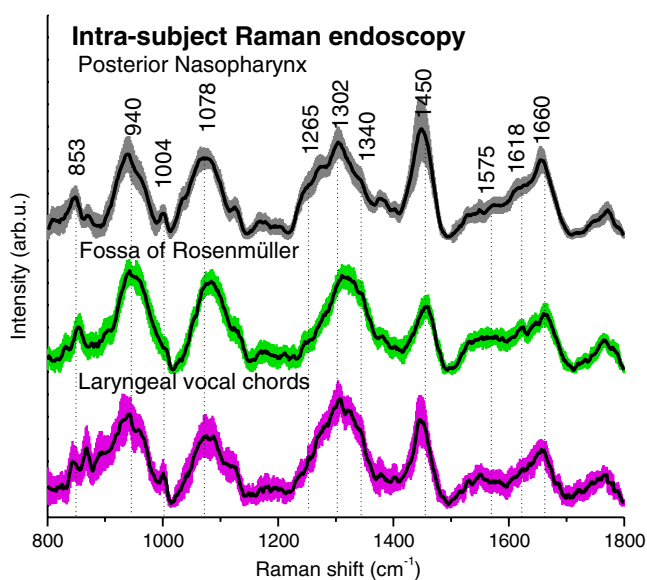

Fig. 1 Representative *in vivo* raw Raman spectrum acquired from FOR with 0.1 s during clinical endoscopic examination. The inset is the processed tissue Raman spectrum after removing the intense autofluorescence background.

Table 1 Tentative assignments[5,11,13,20,30] of molecule vibrations and biochemicals involved in Raman scattering of nasopharyngeal and laryngeal tissue.

Raman peaks (cm⁻¹)	Vibrations	Biochemicals
853	ν(C-C)	Proteins
940	ν(C-C)	Proteins
1004	ν_s(C-C) breathing	Proteins
1078	ν(C-C)	Lipids
1265	Amide III ν(C-N) δ(N-H)	Proteins
1302	CH_2 twisting and wagging	Lipids/proteins
1450	$\delta(CH_2)$	Lipids/proteins
1655	Amide I δ(C = O)	Proteins
1745	ν(C = O)	Phospholipids

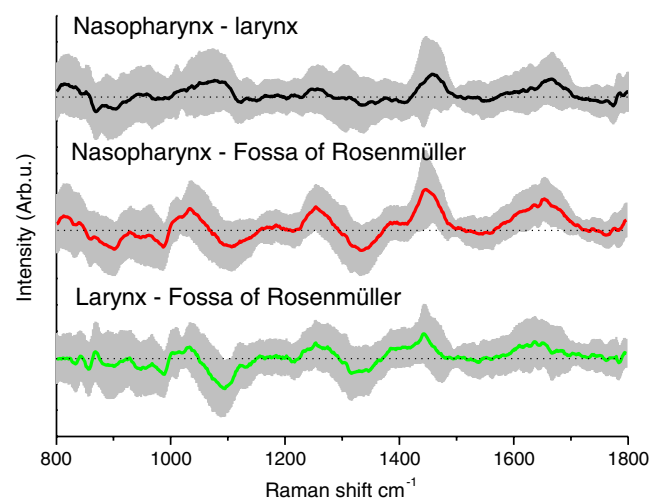Note: ν, stretching mode; ν_s, symmetric stretching mode; δ, bending mode.

4 Discussion

Minimally invasive technologies, such as Raman spectroscopy, can greatly benefit in transnasal inspections of the larynx and nasopharynx in clinical endoscopy. *In vitro* studies have thoroughly demonstrated that NIR Raman spectroscopy is sensitive to carcinogenesis (i.e., precancer and cancer) in the head and neck, including the nasopharynx and larynx.[16–19] Direct translation of this technology into the clinic environment, however, remains very challenging, as efficient fiber probes, short measurement times, and online data processing and diagnosis are needed.[27] This study demonstrates for the first time the feasibility of Raman spectroscopy in transnasal endoscopic applications, providing the foundation for large-scale clinical studies

in the head and neck. Our unique image-guided Raman endoscopy platform, integrated with a miniaturized fiber Raman probe, provides a rapid and minimally invasive assessment of endogenous tissue constituents of the head and neck at the molecular level during clinical endoscopic examination. This greatly facilitates clinicians to obtain detailed biomolecular fingerprints of tissue in the head and neck, reflecting the genuine compositional and morphological signatures without introducing the artifacts caused by vascular puncturing or tissue dehydration, morphological and anatomical effects, etc. Distinct Raman bands near 936 cm⁻¹ [v(C-C) proteins], 1004 cm⁻¹ [ν_s(C-C) ring breathing of phenylalanine], 1078 cm⁻¹ [v(C-C) of lipids], 1265 cm⁻¹ [amide III v(C − N) and δ(N-H) of proteins], 1302 cm⁻¹ [CH_3CH_2 twisting and wagging of proteins], 1450 cm⁻¹ [$\delta(CH_2)$ deformation of proteins and lipids], 1618 cm⁻¹ [v(C = C) of porphyrins], 1655 cm⁻¹ [amide I v(C = O) of proteins] are consistently observed in different anatomical sites of the nasopharynx and larynx

Fig. 3 *In vivo* (intra-subject) mean Raman spectra ±1 SD of PN (*n* = 18), FOR (*n* = 18) and LVCs (*n* = 17). Note that the mean Raman spectra are vertically displaced for better visualization.

Fig. 4 Comparison of difference spectra ±1 SD of different anatomical tissue types (inter- subject): (PN–LVCs); (PN–FOR) and (LVC–FOR).
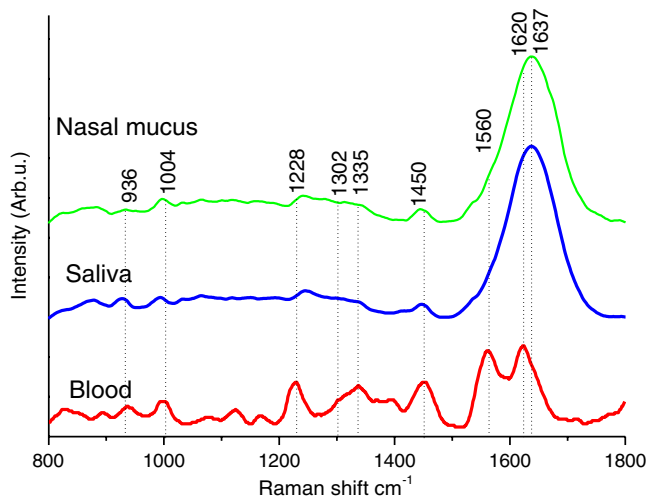
Fig. 5 *In vitro* Raman spectra of possible confounding factors from human body fluids (nasal mucus, saliva, and blood).
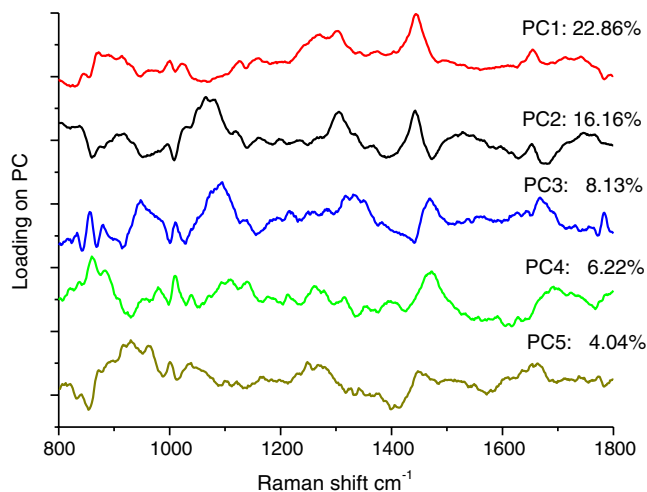

Fig. 6 PC loadings resolving the biomolecular variations among different tissues in the head and neck, representing a total of 57.41% (PC1: 22.86%; PC2: 16.16%; PC3: 8.13%; PC4 6.22% PC5: 4.04%) of the spectral variance.

(Figs. 1 to 3). The difference spectra ±1 SD (Fig. 4) reveal that the Raman-active tissue constituents are comparable among different anatomical sites, but the subtle (while highly molecular-specific) inter-anatomical variations are observed [e.g., relative tissue Raman (spectral shape, bandwidth, peak position and intensity) differences]. With the 785-nm laser light penetration depth in the vicinity of ∼800 μm in epithelial tissue,[12] it is plausible that Raman spectra of nasopharyngeal tissue reflect the lymphoid-rich mucosa and epithelia type (i.e., mostly stratified squamous epithelium). On the other hand, the distinct morphology in the FOR (i.e., cartilage) likely explains the spectral appearance associated with the pharyngeal recess. To investigate further the properties of inter-anatomical variability in the head and neck, PCA was employed to resolve the spectral variability. ANOVA and noise level was used to select the PCs in the model. The PCA modeling captured a total variation of 57.41% after

mean-centering of the dataset (PC1: 22.86%; PC2: 16.16%; PC3: 8.13%; PC4 6.22% PC5: 4.05%) that were found to have significant different means [Fig. 7(a) to 7(e)]. Indeed, this suggests that the majority of the spectral variation is related to inter-anatomical variability. We anticipate that the remaining variance not accounted for is due to probe handling variations associated with *in vivo* Raman endoscopic trials. The loadings on PC1 and PC2 (Fig. 6) are generally associated with lipid signals {i.e., 1302 cm^{-1} (CH$_2$ twisting and wagging), 1440 cm − 1 [δ(CH$_2$)], 1655 cm^{-1} [v(C = C)] and 1745 cm^{-1} [v(C = O)]} suggesting that FOR exhibit fewer signals from lipids (Fig. 7). As both PC1 and PC2 components largely reflect variations in lipids, indicating that distinct lipid types might be associated with the FOR tissues. In contrast, PC3, PC4, and PC5 represent complex signals related to proteins {i.e., 853 cm^{-1} [v(C-C)], 936 cm^{-1} [v(C-C)], 1004 cm^{-1} [v(C-C)], 1450 cm^{-1} [δ(CH$_2$)], and 1660 cm^{-1} [Amide I v(C = O)]}, signifying that distinct anatomical locations are present with a highly specific compositional and morphological signature (Figs. 6 and 7). The two binary PCA-LDA classification algorithms with the LOSO method of cross validation provide the sensitivities of 77.0%, 67.3%, and specificities of 89.2% and 76.0% for differentiation between PN and FOR and between LVC and PN, respectively, reconfirming that the larynx and nasopharynx are unique organs. Therefore, the distinct Raman active biomolecules as well as morphology (e.g., mucosa thickness, cartilage, blood vessels, etc.) and optical properties together contribute to the complex spectral differences observed between different tissue sites in the nasopharynx and larynx. Overall, the subtle spectral differences of distinct anatomical sites observed would inevitably induce additional model complexity in developing efficient Raman diagnostic algorithms [e.g., PCA-LDA, PLS-DA, classification and regression trees (CART), etc.][5,16–19] for precancer and cancer diagnosis in the head and neck. To investigate further the influence of potential confounding factors at *in vivo* transnasal applications, the Raman spectra of body fluids (e.g., blood, saliva, and nasal mucus) in the head and neck were also measured *in vitro* (Fig. 5). Saliva and nasal mucus are mostly associated with broad Raman peak at 1638 cm^{-1} (v_2 bending mode of water), whereas the blood exhibits signals of porphyrins near 1560 and 1620 cm^{-1}. Comparisons with the nasopharyngeal and laryngeal tissue Raman spectra acquired (Fig. 2) reveal that those biochemicals in the body fluids do not contribute significantly to the *in vivo* tissue Raman spectra in transnasal endoscopy.

The *in vivo* nasopharyngeal and laryngeal tissue Raman results presented in this report is of immense importance as it transfers the Raman technology from laboratory into *in vivo*, real-time, transnasal Raman endoscopy, paving the way for realizing early diagnosis and detection of the head and neck cancer and precancer, as well as post-therapeutic surveillance of head and neck cancer during clinical examination.[16–19] One notes that the pharyngeal recess (FOR) could be too deep to be evaluated visually under conventional wide-field imaging modalities (Fig. 2), resulting in blind/random biopsies with poor diagnostic accuracy.[3] Our *in vivo*, fiber-optic Raman endoscopy technique can be used for multiple but instant biochemical assessments of the tissue *in situ* (Fig. 2) that could increase the diagnostic yield and ultimately improve the effectiveness of surveillance of epithelial lesions in the head and neck. Overall, the *in vivo* Raman spectra of the head and neck tissue are very similar, but with subtle spectral differences. This observation correlates
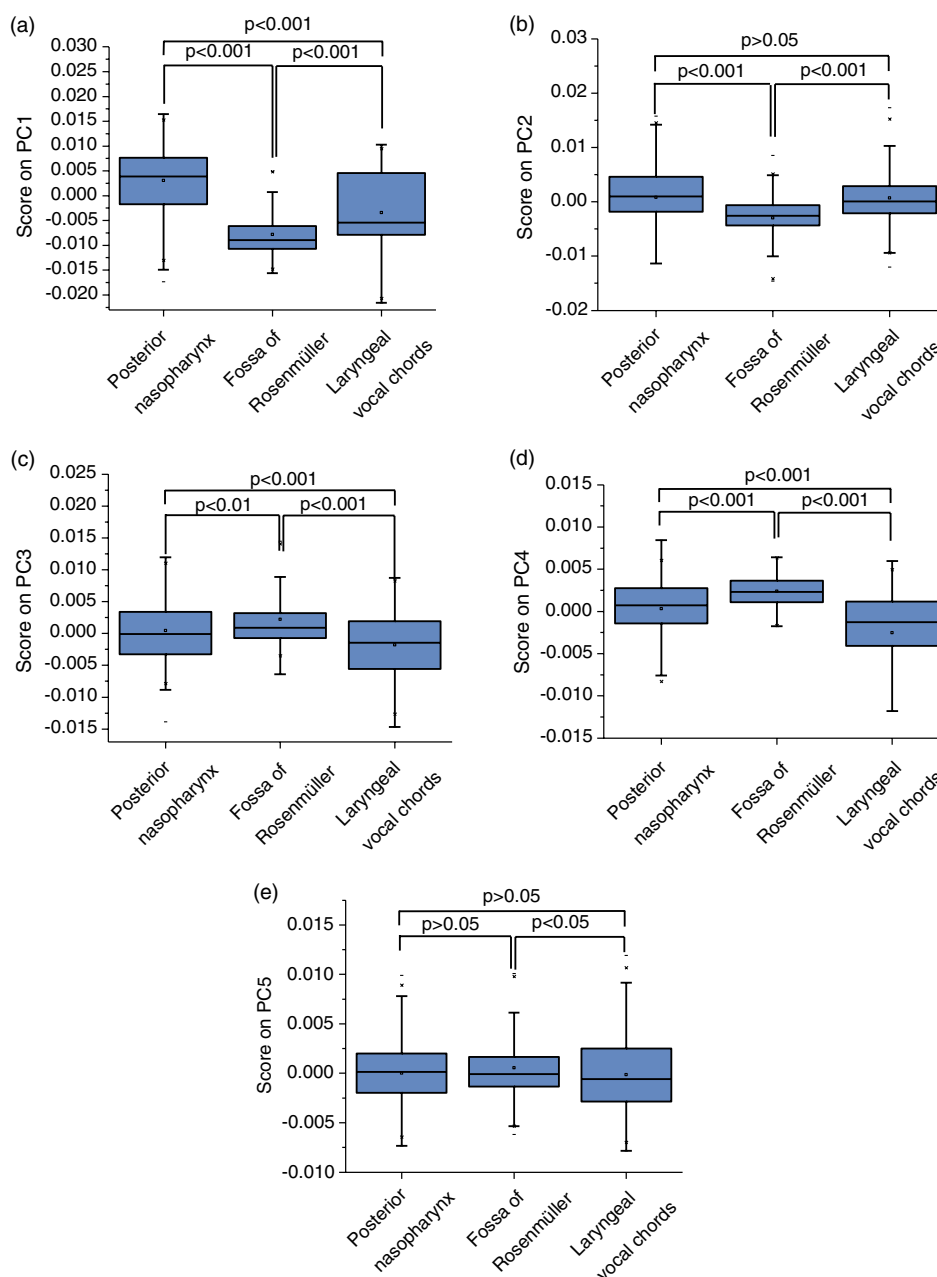
Fig. 7 Box charts of the 5 PCA scores for the different tissue types (i.e., PN, FOR, and LVC). The line within each notch box represents the median, but the lower and upper boundaries of the box indicate the first (25.0% percentile) and third (75.0% percentile) quartiles, respectively. Error bars (whiskers) represent the 1.5-fold interquartile range. The *p*-values are also given among different tissue types.

well with our previous study defining the Raman spectral properties of the upper gastrointestinal tract (i.e., esophagus and gastric).[11] We have also established the Raman spectral profiles of dysplastic and neoplastic tissue in the lung, esophagus, stomach, and colon, which in fact exhibit comparable difference spectra (e.g., cancer tissue shows upregulated DNA and protein, but a relative reduction in lipid content) among different organs associated with neoplastic tissue transformation.[11–13,20,32,33] We anticipate that similar spectral difference profiles could be found in different pathologic tissues of the head and neck, but a large Raman dataset is needed to evaluate the specific impact of cancerous transformation within the distinct anatomical sites in the nasopharynx and larynx. As such, *in vivo*, transnasal Raman endoscopic measurements on a larger number of patients are currently in progress to assess the specific biochemical foundations of the Raman spectral differences between different pathologic types of nasopharynx and larynx tissue for developing robust Raman diagnostic algorithms for *in vivo* tissue diagnostics and characterization in the head and neck.

In summary, this work demonstrates for the first time that transnasal, image-guided Raman endoscopy can be used to acquire *in vivo* Raman spectra from nasopharyngeal and laryngeal tissue in real time. Significant Raman spectral differences are identified, reflecting that the distinct compositions and morphology in the nasopharynx and larynx should be considered to be important parameters in the interpretation and rendering of diagnostic decision algorithms for *in vivo* tissue diagnosis and characterization in the head and neck.

References

1. A. Jemal et al., "Global cancer statistics," *CA: A Cancer J. Clinicians*, **61**(2), 69–90 (2011).
2. L. Döbróssy, "Epidemiology of head and neck cancer: magnitude of the problem," *Cancer Metastasis Rev.* **24**(1), 9–17 (2005).
3. L. E. Loh, T. S. G. Chee, and A. B. John, "The anatomy of the fossa of Rosenmüller—its possible influence on the detection of occult nasopharyngeal carcinoma," *Singapore Med. J.* **32**(3), 154–155 (1991).
4. M. G. Shim et al., "In vivo near-infrared Raman spectroscopy: demonstration of feasibility during clinical gastrointestinal endoscopy," *Photochem. Photobiol.* **72**(1), 146–150 (2000).
5. N. Stone et al., "Raman spectroscopy for identification of epithelial cancers," *Faraday Discuss.* **126**, 141–157 (2004).
6. M. Almond et al., "Raman spectroscopy: a potential tool for early objective diagnosis of neoplasia in the oesophagus," *J. Biophoton.* **4**(10), 685–695 (2011).
7. E. Widjaja, W. Zheng, and Z. Huang, "Classification of colonic tissues using near-infrared Raman spectroscopy and support vector machines," *Int. J. Oncol.* **32**(3), 653–662 (2008).
8. C. Kendall et al., "Raman spectroscopy, a potential tool for the objective identification and classification of neoplasia in Barrett's oesophagus," *J. Pathol.* **200**(5), 602–609 (2003).
9. L. M. Wong et al., "Diagnostic potential of Raman spectroscopy in Barrett's esophagus," *Proc. SPIE* **5692**, 140–146 (2005).
10. I. A. Boere et al., "Use of fiber optic probes for detection of Barrett's epithelium in the rat oesophagus by Raman spectroscopy," *Vib. Spectrosc.* **32**(1), 47–55 (2003).
11. M. S. Bergholt et al., "Characterizing variability of *in vivo* Raman spectra of different anatomical locations in the upper gastrointestinal tract towards cancer detection," *J. Biomed. Opt.* **16**(3), 037003 (2011).
12. M. S. Bergholt et al., "*In vivo* diagnosis of esophageal cancer using image guided Raman endoscopy," *Technol. Cancer. Res. Treat.* **10**(2), 103–112 (2011).
13. Z. Huang et al., "*In vivo* early diagnosis of gastric dysplasia using narrow-band image-guided Raman endoscopy," *J. Biomed. Opt.* **15**(3), 037017 (2010).
14. K. Guze et al., "Parameters defining the potential applicability of Raman spectroscopy as a diagnostic tool for oral disease," *J. Biomed. Opt.* **14**(1), 014016 (2009).
15. A. T. Harris et al., "Raman spectroscopy in head and neck cancer," *Head Neck Oncol.* **2**(26), 1–6 (2010).
16. D. P. Lau et al., "Raman spectroscopy for optical diagnosis in normal and cancerous tissue of the nasopharynx—preliminary findings," *Lasers Surg. Med.* **32**(3), 210–214 (2003).
17. D. P. Lau et al., "Raman spectroscopy for optical diagnosis in the larynx preliminary findings," *Lasers Surg. Med.* **37**(3), 192–200 (2005).
18. S. K. Teh et al., "Spectroscopic diagnosis of laryngeal carcinoma using near-infrared Raman spectroscopy and random recursive partitioning ensemble techniques," *Analyst* **134**(6), 1232–1239 (2009).
19. N. Stone et al., "Raman spectroscopy for early detection of laryngeal malignancy: preliminary results," *Laryngoscope* **110**(10), 1756–1763 (2000).
20. Z. Huang et al., "Near-infrared Raman spectroscopy for optical diagnosis of lung cancer," *Int. J. Cancer* **107**(6), 1047–1052 (2003).
21. A. Mahadevan-Jansen et al., "Near-infrared Raman spectroscopy for in vitro detection of cervical precancers," *Photochem. Photobiol.* **68**(1), 123–132 (1998).
22. J. Mo et al., "High wavenumber Raman spectroscopy for in vivo detection of cervical dysplasia," *Anal. Chem.* **81**(21), 8908–8915 (2009).
23. R. O. P. Draga et al., "*In vivo* bladder cancer diagnosis by high-volume Raman spectroscopy," *Anal. Chem.* **82**(14), 5993–5999 (2010).
24. M. A. Short et al., "Changes in nuclei and peritumoral collagen within nodular basal cell carcinomas via confocal micro-Raman spectroscopy," *J Biomed Opt.* **11**(3), 34004 (2006).
25. K. E. Shafer-Peltier et al., "Raman microspectroscopic model of human breast tissue: Implications for breast cancer diagnosis in vivo," *J. Raman Spectrosc.* **33**(7), 552–563 (2002).
26. A. S. Haka et al., "*In vivo* margin assessment during partial mastectomy breast surgery using Raman spectroscopy," *Cancer Res.* **66**(6), 3317–3322 (2006).
27. Z. Huang et al., "Integrated Raman spectroscopy and trimodal widefield imaging techniques for real-time *in vivo* tissue Raman measurements at endoscopy," *Opt. Lett.* **34**(6), 758–760 (2009).
28. Z. Huang et al., "Rapid near-infrared Raman spectroscopy system for real-time *in vivo* skin measurements," *Opt. Lett.* **26**(22), 1782–1784 (2001).
29. American National Standard for the Safe Use of Lasers: ANSI Standard 2136.1-1986 American National Standards Institute, Washington, D.C. (1986).
30. A. Mahadevan-Jansen and R. Richards-Kortum, "Raman spectroscopy for the detection of cancers and precancers," *J. Biomed. Opt.* **1**(1), 31–70 (1996).
31. N. Stone et al., "Near-infrared Raman spectroscopy for the classification of epithelial pre-cancers and cancers," *J. Raman Spectrosc.* **33**(7), 564–573 (2002).
32. R. W. Short et al., "Raman spectroscopy detects biochemical changes due to proliferation in mammalian cell cultures," *Biophys. J.* **88**(6), 4274–4288 (2005).
33. K. Lin, D. P. Lau, and Z. Huang, "Optical diagnosis of laryngeal cancer using high wavenumber Raman spectroscopy," *Biosens. Bioelectron.* **35**(1), 213–217 (2012).